# Velocity of vertical fluid ascent within vein-forming fractures



doi: 10.1130/G25680A.1

Geology

# Velocity of vertical fluid ascent within vein-forming fractures

Atsushi Okamoto and Noriyoshi Tsuchiya

*Geology* 2009;37;563-566
doi: 10.1130/G25680A.1



**Notes**



# Velocity of vertical fluid ascent within vein-forming fractures

Atsushi Okamoto* and Noriyoshi Tsuchiya
Graduate School of Environmental Studies, Tohoku University, Sendai 980-8579, Japan

## ABSTRACT

**Quartz-albite-calcite veins in metamorphic rocks of the Sanbagawa belt, Japan, contain sugary mosaics of equant quartz grains <0.01–1.6 mm in size (blocky texture). The quartz crystals show euhedral to subhedral double-terminated crystal shape, and concentric growth zoning, indicating suspension in aqueous fluid during crystal growth until formation of a framework within the crack. Such a crystallization process is only possible when downward crystal settling is balanced by upward fluid flow. Application of crystal settling theory to the crystal size distributions within the veins reveals an extremely high rate of fluid ascent during blocky vein formation ($10^{-2}$ to $10^{-1}$ m/s) due to the low viscosity of the hydrothermal fluid (~$10^{-4}$ Pa·s). Such a high rate of ascent suggests the injection of fluids from mobile hydrofractures within deeper levels of the subduction zone.**

## INTRODUCTION

The generation and transport of aqueous fluids play a significant role in subduction zone volcanism, seismicity, and metamorphism and in global material circulation (Hacker et al., 2003). At intermediate and shallow crustal levels, fractures and faults play a dominant role in controlling fluid flow (Oliver, 1996); however, the rate of fluid flow remains poorly understood. Veins provide information on the nature of the fluid-filled cracks from which they evolved. One of the fundamental constraints on fluid flow during vein formation is the time-integrated fluid flux, which can be estimated from the total vein mass and the solute concentration in fluids (Bons, 2001); however, it is generally difficult to accurately determine fluid compositions. Even if the total fluid flux is known, the flow rate and time scale of crack sealing cannot be independently determined. In addition, vein formation occurs even in stagnant fluids by molecular diffusion (Fisher and Brantley, 1992).

In this paper, we investigate the crystal shape, growth pattern, and crystal size distributions (CSDs) of blocky quartz veins that developed during exhumation of the Sanbagawa metamorphic belt, which contains accretionary rocks from a subduction zone. Here, blocky texture indicates mosaics of equant grains within veins. We apply crystal settling theory to constrain the rate of fluid ascent during vein formation within the subduction zone.

We present textural evidence of fluid movement in cracks based on analyses of veins in low-grade metamorphic rocks. In general, mineral crystallization within fluid-filled cracks occurs by three mechanisms (e.g., Oliver and Bons, 2001): (1) epitaxial growth on the surfaces of preexisting minerals of the same species along the crack wall, producing fibrous, elongate-blocky, and stretched-crystal veins; (2) heterogeneous nucleation on preexisting minerals and growth, producing antiaxial fibrous veins; and (3) homogeneous nucleation and subsequent overgrowth in fluids, producing blocky veins. During the formation of blocky veins, crystals growing in fluids should be dynamically affected by fluid flow and gravity, analogous to such effects in crystallization in a magma chamber or conduit.

## GEOLOGICAL SETTING AND VEIN OCCURRENCE

The Sanbagawa belt is a Cretaceous high-pressure metamorphic belt that extends over a distance of 700 km throughout the Japanese Islands. The belt is dominated by metasediments and metabasalt that were originally part of a subducting oceanic slab. These rocks record metamorphism in the greenschist, epidote-amphibolite, and eclogite facies (Enami et al., 1994; Aoya, 2003), involving the subduction of a young, warm slab (Aoya, 2003). Schists of the Sanbagawa belt contain a prominent east-west–striking subhorizontal stretching lineation developed during exhumation in response to extension parallel to the paleotrench axis (Wallis, 1998).

In the Nagatoro area of the Kanto Mountains, veins in rocks of the chlorite zone are commonly subvertical, intersecting the foliation and the stretching lineation within the host rocks at a high angle (60°–90°). Petrological and fluid-inclusion studies reveal that these veins formed at 200–400 °C and 0.1–0.4 GPa, during the late stages of exhumation of the Sanbagawa belt (Okamoto et al., 2008). Because the fold axes of exhumation-related upright folds are oriented normal to the high-angle veins, it is likely that the veins formed vertically.

The high-angle veins are classified into two types: (1) quartz-albite-chlorite-K-feldspar (Qtz-Ab-Chl-Kfs) veins that show stretched-crystal to elongate-blocky textures, and constitute more than 70% of veins in the area, and (2) quartz-albite-calcite (Qtz-Ab-Cal) veins with blocky textures (Morohashi et al., 2008; Okamoto et al., 2008). Qtz-Ab-Cal veins cut Qtz-Ab-Chl-Kfs veins and vice versa, indicating their crack development over the same time interval, but Qtz-Ab-Cal veins are generally thicker and longer than Qtz-Ab-Chl-Kfs veins. Based on the pattern of mineral distribution within the veins and crack aperture, Okamoto et al. (2008) proposed that the chemical components of the Qtz-Ab-Chl-Kfs veins were derived from adjacent host rocks, whereas those of the Qtz-Ab-Cal veins were derived from distant sites.

## METHOD

Microstructural observations were made from four Qtz-Ab-Cal veins in thin sections cut normal to the vein wall, using an optical microscope and scanning electron microscope equipped to detect cathodoluminescence (SEM-CL). The outlines of quartz crystals were manually traced on optical photomicrographs and X-ray maps of Si compiled using an electron probe microanalyzer (JEOL 8200, University of Tokyo); crystal diameters were measured as $L = 2 \times (\text{area}/\pi)^{1/2}$. The resolution of the analyzed images enabled measurements for crystals larger than 10 μm. The two-dimensional CSDs were converted to three-dimensional CSDs following the stereological approach proposed by Sahagian and Proussevitch (1998), under the assumption of spherical crystal shape.

## VEIN TEXTURES AND INTERPRETATION

The examined Qtz-Ab-Cal veins, 5–100 mm thick and 1–10 m long, commonly contain several wall-parallel laminations of 0.5–5 mm thickness (Fig. 1A). Individual layers are distinguished by mineral mode and crystal size, and layers are separated by sharp boundaries. The mineral mode varies markedly among individual veins and wall-parallel layers, ranging from quartz-dominant (Qtz > 90 vol%) to albite-dominant (Ab > 60 vol%). The calcite mode is generally less than 20 vol%. These textures indicate multiple crack-seal events in response to influxes of external fluids with contrasting compositions (Okamoto et al., 2008).

The size of quartz crystals in the veins commonly ranges from <10 to 500 μm. Some veins contain euhedral to subhedral quartz crystals with hexagonal outlines (Figs. 1B–1E). The aspect ratio (length/width) of quartz crystals is commonly 1–3, and the mean value is 1.5–1.7 (Table 1). Growth zoning in quartz is indicated by concentric inclusion

*E-mail: okamoto@mail.kankyo.tohoku.ac.jp.

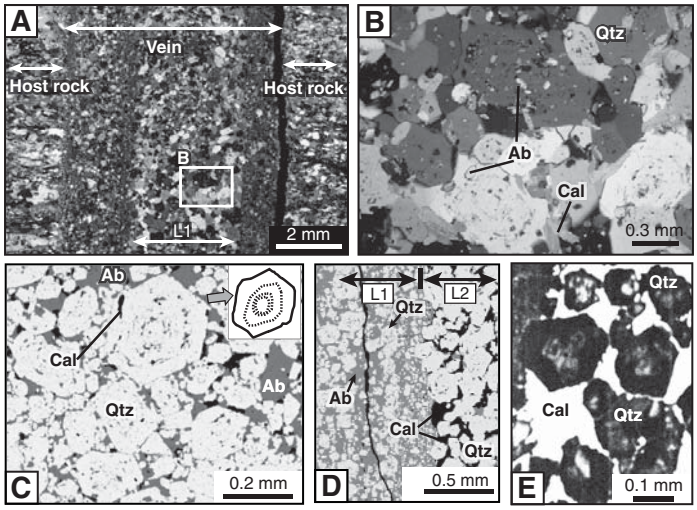


**Figure 1. Representative images of microstructures within Qtz-Ab-Cal veins from the Sanbagawa schists. A: Optical photomicrograph of a vein (sample 10D-L1, vertical section) under polarized light. White rectangle indicates the area shown in B. B: Optical photomicrograph of the region indicated by the white rectangle in A. C: X-ray map of Si concentrations (sample 11-L2, horizontal section) accompanying sketch of concentric growth zoning of a quartz crystal. D: X-ray map of Si concentrations (samples 11-L1 and 11-L2, vertical section). E: SEM-CL image of a vein (sample 10D-L1, vertical section). Qtz—quartz; Ab—albite; Cal—calcite.**

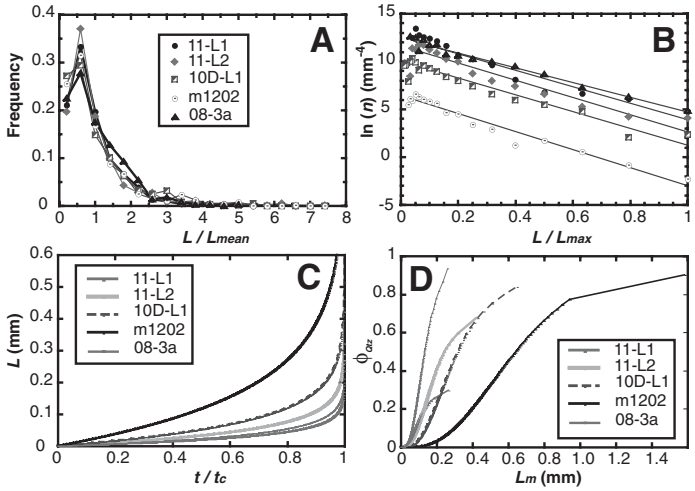


**Figure 2. A: Two-dimensional CSDs of quartz crystals within the analyzed veins. The crystal size, *L*, is normalized by the geometric mean, $L_{mean}$ (see Table 1). B: Three-dimensional CSDs of quartz crystals converted from two-dimensional CSDs. *L* is normalized by the largest crystal size in each sample, $L_{max}$, and each geometric size class is defined as being $10^{-0.1}$ times the last (Sahagian and Proussevitch, 1998). The fitting lines were calculated using the least squares method, and data points for the smaller size classes were excluded due to the insufficient resolution of the images. C: Evolution of crystal size (as calculated by Equation 3), using $L_0 = 10^{-6}$ mm and measured values of *S* and $L_{max}$ (see Table 1). At $t/t_c = 1$, the crystal size reaches $L_{max}$. D: Temporal evolution of the volume fraction of quartz. The largest crystal size, $L_m$, at each time is used as the indicator of time.**

TABLE 1. CHARACTERISTICS OF Qtz-Ab-Cal VEINS

| Sample number | 11-L1 | 11-L2 | 10-1D3 | m1202 | 08-3a |
|---|---|---|---|---|---|
| Analyzed area (mm$^2$) | 3.94 | 2.56 | 7.77 | 36.2 | 2.1 |
| Number of measured crystals | 816 | 507 | 661 | 476 | 440 |
| Geometric mean, $L_{mean}$ (mm) | 0.024 | 0.035 | 0.056 | 0.130 | 0.039 |
| $L_{max}$ (mm) | 0.267 | 0.421 | 0.647 | 1.584 | 0.260 |
| Quartz modal abundance, $M_{Qtz}$ | 0.30 | 0.67 | 0.84 | 0.90 | 0.93 |
| Quartz mean aspect ratio | 1.58 | 1.63 | 1.66 | 1.59 | 1.67 |
| Slope in *L*-ln(*n*) plot, *S* | –36.6 | –21.5 | –13.5 | –5.9 | –29.4 |

trails of albite and calcite (Figs. 1B and 1C) and core-mantle structures with contrasting CL intensities, as observed in SEM-CL images (Fig. 1E). Such quartz textures are found in both horizontal and vertical sections of the same vein (Figs. 1C and 1D), indicating double-terminated crystal shape. The pores between quartz crystals are filled with fine-grained albite (<10 μm) and anhedral calcite. The occurrence of albite and calcite suggests their continuous crystallization during and after quartz crystallization. Euhedral crystal faces of quartz are preferentially preserved at contacts with albite or calcite (Figs. 1C–1E); in contrast, concavo-convex and irregular boundaries occur at quartz-quartz contacts (Fig. 1B), indicating that quartz grains impinged on each other during crystallization and that modification of some grain boundaries occurred after crystallization.

We measured the CSDs of quartz crystals in four veins (Table 1). Different wall-parallel layers in individual veins (layers L1 and L2 within sample 11) are treated as separate veins. Despite variations in mineral modes and mean crystal sizes (Table 1), all two-dimensional CSDs show similar patterns (Fig. 2A), in which the frequency of quartz crystals increases markedly with decreasing crystal size. The frequency drop at the smallest size class is probably a reflection of the resolution of the analyzed images. The three-dimensional CSDs shown in an $L/L_{max}$-ln(*n*) plot define linear trends with negative slopes (Fig. 2B), where *n* is the number density of quartz crystals (crystals per unit volume per size, mm$^{-4}$). The slopes of these trends, *S*′, can be converted to the slopes of *L*-ln(*n*) plots, *S*, following the relation $S = S'/L_{max}$. The obtained *S* values range from –5.9 to –36.6 (Table 1). The trend and slope of CSDs do not change significantly, even when we assume crystal shapes to be prolate rotational ellipsoids with aspect ratio of 1.5.

Linear CSD trends in *L*-ln(*n*) plots have been modeled as crystallization in batch or open magmatic systems (e.g., Marsh, 1988, 1998). These trends suggest (1) continuous nucleation and growth during crystallization, and (2) small physical effects including crystal accumulation (or fractionation), which yields concave-upward (or downward) curvature (Marsh, 1988). As the simplest case, we consider a fluid-filled crack that resembles a batch system, where generated crystals remain but fluid can pass through the crack, because the veins commonly show lenticular shapes with length less than 10 m. Linear CSD trends obtained for a batch system can be explained by two crystallization models: (1) exponentially increasing nucleation rate with time and constant growth rate (Marsh, 1998), and (2) constant nucleation rate and size-dependent growth rate (Eberl et al., 1998; Marsh, 1998). The former model is applicable to crystallization within a magma chamber, in which case the saturation level increases with continuous cooling; however, the applicability to hydrothermal veins is not clear. The size-dependent growth has been reported for crystallization in natural and experimental environments (e.g., Eberl et al., 1998). A simple expression of the size-dependent growth rate, $dL/dt = G$, is

$$G = G_0 \exp(-SL) \quad (1)$$

where *S* is the slope in an *L*-ln(*n*) plot and $G_0$ is a pre-exponential factor (Marsh, 1998). Integrating Equation 1, we obtain the evolution of crystal size, *L*, as follows:

$$L(t) = (1/S)\ln[G_0 t + B] \quad (2)$$

where $B$ is a constant. When the crystal size is $L_0$ at $t = 0$ (nuclei size), and is $L_{max}$ at the time when crystallization was completed ($t = t_c$), Equation 2 is rewritten as

$$L(t/t_c) = (L_{max}/S)\ln\left\{\left[\exp(S) - \exp(SL_0/L_{max})\right]t/t_c + \exp(SL_0/L_{max})\right\} \quad (3)$$

where $t/t_c$ takes values ranging from 0 to 1. According to this model with assumption of $L_0 = 10^{-6}$ mm, the crystal size increases markedly during the late stages of crystallization ($t/t_c > 0.8$; Fig. 2C). Assuming a constant nucleation rate and spherical crystal shape, the evolution of the quartz crystal fraction, $\phi_{Qtz}$, is obtained using $\phi_{Qtz\,(t=0)} = 0$ and $\phi_{Qtz\,(t=tc)} = M_{Qtz}$, where $M_{Qtz}$ is the modal abundance of quartz measured in thin section (Table 1). In Figure 2D, the temporal evolution of $\phi_{Qtz}$ is plotted against the largest crystal size at each time, $L_m$. The quartz crystal fraction increased with increasing $L_m$, and all the $L_m$-$\phi_{Qtz}$ plots are characterized by sigmoidal trends.

## TERMINAL VELOCITY OF QUARTZ CRYSTALS

Given the homogeneous nucleation and growth of quartz crystals in a static fluid within a crack, crystals are expected to move downward to the crack base or wall due to the large density difference between quartz crystals and the host aqueous fluid (Fig. 3A). Once the quartz crystals have settled to the bottom of the crack, quartz would preferentially overgrow the crystal surface in contact with the fluid. This crystal settling and subsequent growth should form anisotropic growth zoning and irregular grain shapes (Fig. 3A); thus, the textures observed in the analyzed veins (Fig. 1) were not produced in a static fluid. In contrast, double-terminated quartz crystals with concentric growth zoning can develop in crystal-fluid suspensions subjected to upward fluid flow (Fig. 3B), where the drag imposed by the upward-moving fluid balances the downward-moving effect of the weight of immersed quartz crystals (Allen, 1985). In a fluid-filled crack including crystals with various sizes, all crystals are suspended and move upward when the upward fluid flow rate is greater than the terminal velocity of the largest crystal; this process is like that in fluidized beds (Oliver et al., 2006).

Here, we consider vein formation at 300 °C and 0.25 GPa (Okamoto et al., 2008), at which the density and viscosity of water are $\rho_{H_2O} = 0.91$ g/cm$^3$ (Holland and Powell, 1991) and $\mu_f = 1.3 \times 10^{-4}$ Pa·s (International Association for the Properties of Water and Steam, 2008), respectively. The density of quartz is taken to be 2.65 g/cm$^3$. The terminal velocity of a solitary spherical rigid particle, $V_0$, in a stagnant fluid is written as $V_0 = [4(\rho_d - \rho_f)gL/(3C_D\rho_f)]^{1/2}$ (Allen, 1985). $L$, $\rho_d$, $\rho_f$, and $g$ are particle diameter, particle density, fluid density, and gravitational acceleration, respectively. $C_D$ is the drag coefficient for a solitary spherical particle and is empirically expressed as functions of the particle Reynolds number, $Re = \rho_f LV_0/\mu_f$ (Clift et al., 1978). When the particle Reynolds number is less than 1.0, the terminal velocity follows Stokes' law, $V_0 = (\rho_d - \rho_f)gL^2/18\mu_f\rho_f$. Figure 4A shows the terminal velocity of a single spherical quartz crystal,

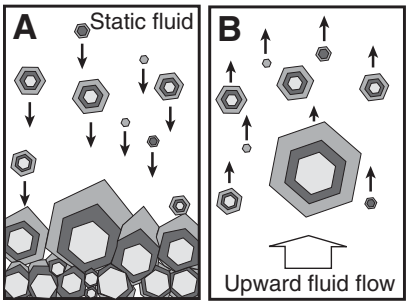


**Figure 3. Schematic models showing crystal growth in a vertical fluid-filled crack. Individual growth stages are shown by different colors, and black arrows indicate direction of crystal movement. A: In a static fluid, crystals settle on the crack bottom, and form anisotropic growth zoning. B: In crystal-fluid suspension subjected to upward fluid flow, quartz crystals form concentric growth zoning. Crystals travel upward when fluid flow rate is higher than terminal velocity of crystal.**

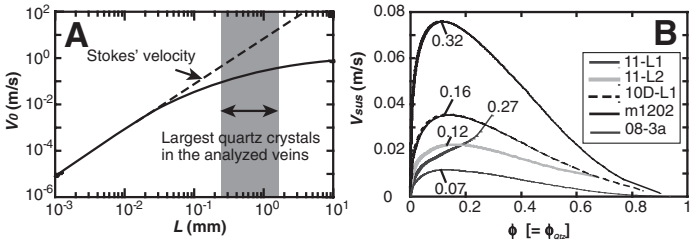


**Figure 4. A: Terminal velocity of a single quartz crystal in water at 300 °C and 250 MPa (solid curve). Dashed curve indicates Stokes' velocity. B: Temporal evolution of the terminal velocity of the largest crystal in a crack, $V_{sus}$, with respect to the volume fraction of crystals, $\phi$ (= $\phi_{Qtz}$). The relationship between $L_m$ and $\phi_{Qtz}$ is shown in Figure 2D.**

$V_0$, in an aqueous fluid. $V_0$ increases from $10^{-5}$ to ~1 m/s with increasing crystal size from $10^{-3}$ to 10 mm, and deviates from Stokes' velocity at $L > 0.03$ mm. For the largest crystal sizes in the analyzed veins (0.27–1.58 mm), $V_0$ ranges from 0.09 to 0.30 m/s. These values provide a convincing limit on upward fluid flow rate required for crystal-fluid suspension, but it is necessary to consider the effect of crystal fraction within a crack, $\phi$, which increases during crystallization (Fig. 2D).

The terminal velocity of the particles in the arrays, $V_{sus}$, decreases with increasing $\phi$, according to $V_{sus} = (1 - \phi)^{\alpha}V_0$, where $\alpha$ is a positive exponent ranging from 2.33 to 4.65, related to the particle Reynolds number (Shaw, 1965; Allen, 1985). The above relation is valid for $\phi < 0.6$ until the crystals form a solid framework ($\phi > 0.6$–$0.74$). To investigate the upward fluid flow velocity required for the crystal-fluid suspensions throughout the crystallization history, we evaluated the terminal velocity in the crystal arrays, $V_{sus}$, for the largest crystal size, $L_m$, at each time (Fig. 4B), using the $L_m$-$\phi_{Qtz}$ relation shown in Figure 2D and the assumption that $\phi = \phi_{Qtz}$. Except for one sample with a minor quartz mode, 11-L1, the model predicts that the highest upward fluid velocities (0.01–0.08 m/s) are required at the intermediate stage of crystallization ($\phi = 0.1$–$0.2$), because crystal growth led to an increase in settling velocity during the initial stages of crystallization, whereas the effect of crystal fraction on settling velocity becomes predominant during later stages. The observed textures are similar to those seen in plutonic rocks, but a high fluid flow rate on the order of $10^{-2}$ to $10^{-1}$ m/s was required because of the low viscosity of aqueous fluids (~$10^{-4}$ Pa·s) compared with that of melts ($10^5$ to $10^{10}$ Pa·s).

## DISCUSSION

Blocky veins are common in various geological settings related to ore mineralization (e.g., Rusk and Reed, 2002), seismicity (e.g., Lee and Wiltschko, 2000), and igneous and metamorphic events (Bons, 2001); these veins are considered to form under advective flow regimes rather than by diffusive material transport (Oliver and Bons, 2001; Okamoto et al., 2008). Few studies have sought to constrain the rate of fluid flow during blocky vein formation, because primary crystal shapes are commonly modified by annealing and/or dynamic recrystallization subsequent to vein crystallization. The veins analyzed in the present study are relatively undeformed, and the quartz crystals are surrounded by other mineral species, thereby retaining euhedral crystal shapes and growth zoning. Even for blocky veins affected by recrystallization, growth zoning and the framework structures of quartz crystals can be observed by SEM-CL imaging (Rusk and Reed, 2002; Jessell et al., 2003); the detailed analyses of these textures provide significant information on fluid movement.

The Qtz-Ab-Cal veins record the influx of external fluids, probably from dehydration of the subducting slab and sediments beneath the Sanbagawa belt during exhumation (Okamoto et al., 2008). The results of the present study suggest the fluid ascent rate could be very high ($10^{-2}$ to

$10^{-1}$ m/s) within certain cracks generated within a subduction zone. It is unclear whether the rate can be realized by (1) fluid flow through fracture networks, or (2) fluid ascent by buoyancy-driven propagation of isolated fluid-filled fractures (mobile hydrofracture; e.g., Nakashima, 1993; Dahm, 2000; Bons, 2001; Oliver and Bons, 2001). The Sanbagawa veins occur as isolated lenses with lengths of <10 m and do not appear to form kilometer-scale fracture networks; thus, the latter mechanism is more likely than the former. The mobile hydrofracture model predicts that fluid batches for fracture lengths of 50–100 m and widths of 0.01–0.1 mm can ascend at velocities of 0.1–1 m/s under crustal conditions (Nakashima, 1993), but that the geometries of the present veins (length = 1–10 m; width = 0.5–5 mm) would preclude crack movement. This suggests that the observed Qtz-Ab-Cal veins do not show the original shape of propagating fluid-filled cracks, but represent indicators of failed fluid flow or arrest probably due to the leak of fluids and the increase of crystal fraction at the final emplacement depth (Bons, 2001). We speculate that the crystallization within these veins occurred within stationary cracks by the episodic injection of fluids derived from upward-moving mobile hydrofractures. The high ascent rate of fluids could realize both the high $SiO_2$ concentrations required for nucleation and the development of crystal-fluid suspension. Nuclei formed in deeper parts could be brought with fluid toward shallower depths.

**ACKNOWLEDGMENTS**

We thank T. Kuwatani for assistance with electron probe microanalyses, K. Morohashi for help in the field, M. Toriumi for useful discussions, and P.D. Bons, N.H.S. Oliver, and M.H. Reed for extensive reviews. This study was supported by a grant from the Japan Society for the Promotion of Science (No. 18740317) awarded to A. Okamoto.

**REFERENCES CITED**

Allen, J.R.L., 1985, Principles of physical sedimentology: Caldwell, New Jersey, Blackburn Press, 272 p.

Aoya, M., 2003, Subduction-stage pressure path of eclogite from the Sambagawa belt: Prophetic record for oceanic-ridge subduction: Geology, v. 31, p. 1045–1048, doi: 10.1130/G19927.1.

Bons, P.D., 2001, The formation of large quartz veins by rapid ascent of fluids in mobile hydrofractures: Tectonophysics, v. 336, p. 1–17, doi: 10.1016/S0040-1951(01)00090-7.

Clift, R., Grace, J.R., and Weber, M.E., 1978, Bubbles, drops and particles: New York, Academic Press, p. 369.

Dahm, T., 2000, On the shape and velocity of fluid-filled fractures in the Earth: Geophysical Journal International, v. 142, p. 181–192, doi: 10.1046/j.1365-246x.2000.00148.x.

Eberl, D.D., Drits, V.A., and Srodon, J., 1998, Deducing growth mechanisms for minerals from the shapes of crystal size distributions: American Journal of Science, v. 298, p. 499–533.

Enami, M., Wallis, S.R., and Banno, Y., 1994, Paragenesis of sodic pyroxene-bearing quartz schists: Implications for the *P-T* history of the Sanbagawa belt: Contributions to Mineralogy and Petrology, v. 116, p. 182–198, doi: 10.1007/BF00310699.

Fisher, D.M., and Brantley, S.L., 1992, Models of quartz overgrowth and vein formation: Deformation and episodic fluid flow in an ancient subduction zone: Journal of Geophysical Research, v. 97, p. 20,043–20,061, doi: 10.1029/92JB01582.

Hacker, B.R., Abers, G.A., and Peacock, S.M., 2003, Subduction factory, 1: Theoretical mineralogy, densities, seismic wave speeds, and $H_2O$ contents: Journal of Geophysical Research, v. 108, no. B1, 2029, doi: 10.1029/2001JB001127.

Holland, T., and Powell, R., 1991, A compensated-Redlich-Kwong (CORK) equation for volumes and fugacities of $CO_2$ and $H_2O$ in the range 1 bar to 50 kbar and 100–1600 °C: Contributions to Mineralogy and Petrology, v. 109, p. 265–273, doi: 10.1007/BF00306484.

International Association for the Properties of Water and Steam, 2008, Revised release on the IAPA Formulation 1985 for the viscosity of ordinary water: http://www.iapws.org/relguide/visc.pdf#search=%27viscosity%20of%20water,%20IAPWS (April 2008).

Jessell, M.W., Kostenko, O., and Jamtveit, B., 2003, The preservation potential of microstructures during static grain growth: Journal of Metamorphic Geology, v. 21, p. 481–491, doi: 10.1046/j.1525-1314.2003.00455.x.

Lee, Y.-J., and Wiltschko, D.V., 2000, Fault controlled sequential dilation: Competition between slip and precipitation rates in the Austin Chalk, Texas: Journal of Structural Geology, v. 22, p. 1247–1260, doi: 10.1016/S0191-8141(00)00045-6.

Marsh, B.D., 1988, Crystal size distribution (CSD) in rocks and the kinetics and dynamics of crystallization: Contributions to Mineralogy and Petrology, v. 99, p. 277–291, doi: 10.1007/BF00375362.

Marsh, B.D., 1998, On the interpretation of crystal size distributions in magmatic systems: Journal of Petrology, v. 39, p. 553–599, doi: 10.1093/petrology/39.4.553.

Morohashi, K., Okamoto, A., Satish-Kumar, M., and Tscuchiya, N., 2008, Variation in stable isotope compositions ($\delta^{13}C$, $\delta^{18}O$) of calcite within exhumation-related veins from the Sanbagawa metamorphic belt: Journal of Mineralogical and Petrological Sciences, v. 103, p. 361–364, doi: 10.2465/jmps.080620b.

Nakashima, Y., 1993, Buoyancy-driven propagation of an isolated fluid-filled crack in rock: Implication for fluid transport in metamorphism: Contributions to Mineralogy and Petrology, v. 114, p. 289–295, doi: 10.1007/BF01046532.

Okamoto, A., Kikuchi, T., and Tsuchiya, N., 2008, Mineral distribution within polymineralic veins in the Sanbagawa belt, Japan: Implications for mass transfer during vein formation: Contributions to Mineralogy and Petrology, v. 156, p. 323–336, doi: 10.1007/s00410-008-0288-y.

Oliver, N.H.S., 1996, Review and classification of structural controls on fluid flow during regional metamorphism: Journal of Metamorphic Geology, v. 14, p. 477–492, doi: 10.1046/j.1525-1314.1996.00347.x.

Oliver, N., and Bons, P., 2001, Mechanisms of fluid flow and fluid-rock interaction in fossil metamorphic hydrothermal systems inferred from vein-wall-rock patterns, geometry and microstructure: Geofluids, v. 1, p. 137–162, doi: 10.1046/j.1468-8123.2001.00013.x.

Oliver, N.H.S., Rubenach, M.J., Fu, B., Baker, T., Blenkinsop, T.G., Cleverley, J.S., Marshall, L.J., and Ridd, P.J., 2006, Granite-related overpressure and volatile release in the mid crust: Fluidized breccias from the Cloncurry District, Australia: Geofluids, v. 6, p. 346–358, doi: 10.1111/j.1468-8123.2006.00155.x.

Rusk, B., and Reed, M., 2002, Scanning electron microscope–cathodoluminescence analysis of quartz reveals complex growth histories in veins from the Butte porphyry copper deposit, Montana: Geology, v. 30, p. 727–730, doi: 10.1130/0091-7613(2002)030<0727:SEMCAO>2.0.CO;2.

Sahagian, D.L., and Proussevitch, A.A., 1998, 3D particle size distributions from 2D observations: Stereology for natural applications: Journal of Volcanology and Geothermal Research, v. 84, p. 173–196, doi: 10.1016/S0377-0273(98)00043-2.

Shaw, H.R., 1965, Comments on viscosity, crystal settling and convection in granitic magmas: American Journal of Science, v. 263, p. 120–152.

Wallis, S., 1998, Exhuming the Sanbagawa metamorphic belt: The importance of tectonic discontinuities: Journal of Metamorphic Geology, v. 16, p. 83–95, doi: 10.1111/j.1525-1314.1998.00072.x.

Manuscript received 18 November 2008
Revised manuscript received 5 February 2009
Manuscript accepted 6 February 2009

Printed in USA